Hindawi Publishing Corporation
Science and Technology of Nuclear Installations
Volume 2014, Article ID 602062, 9 pages
http://dx.doi.org/10.1155/2014/602062

Research Article

Influence of Spacer Grid Outer Strap on Fuel Assembly Thermal Hydraulic Performance

Jingwen Yan, Yuxiang Zhang, Baowen Yang, Weicai Li, and Yuemin Zhou

Nuclear Fuel Research and Development Center, China Nuclear Power Technology Research Institute, Shenzhen 518026, China

Correspondence should be addressed to Jingwen Yan; yanjingwen@cgnpc.com.cn

Received 10 October 2013; Accepted 24 December 2013; Published 11 February 2014

Academic Editor: Jianqiang Shan

Copyright © 2014 Jingwen Yan et al. This is an open access article distributed under the Creative Commons Attribution License, which permits unrestricted use, distribution, and reproduction in any medium, provided the original work is properly cited.

The outer strap as a typical structure of a spacer grid enhances the mechanical strength, decreases hang-up susceptibility, and also influences thermal hydraulic performance, for example, pressure loss, mixing performance, and flow distribution. In the present study, a typical grid spacer with different outer strap designs is adopted to investigate the influence of outer strap design on fuel assembly thermal hydraulic performance by using a commercial computational fluid dynamics (CFD) code, ANSYS CFX, and a subchannel analysis code, FLICA. To simulate the outer straps' influence between fuel assemblies downstream, four quarter-bundles from neighboring fuel assemblies are constructed to form the computational domain. The results show that the outer strap design has a major impact on cross-flow between fuel assemblies and temperature distribution within the fuel assembly.

1. Introduction

Most of PWRs consist of 17 × 17 nuclear fuel assemblies that are supported by structural grids over the length of each particular assembly. Spacer grids are used to hold fuel rod bundles in position, maintain appropriate rod-to-rod clearance, and enhance critical heat flux. The outer strap as a typical structure of a spacer grid plays a very important role in enhancing the mechanical strength, decreasing hang-up susceptibility, and also influencing thermal hydraulic performance, for example, pressure loss, mixing performance, and flow distribution. However, it is difficult to carry out the related experiments to investigate these thermal hydraulic characteristics within rod-bundle-grids. Despite the great improvement of experimental technique, the experimental investigations are still expensive and require a relative long time to perform. Computational fluid dynamics (CFD) methodology then attracts more attention from the academic and industry society to simulate these complicated phenomena, including the cross-flow between bundle, mixing, and flow distributions.

Several studies have been carried out on flow mixing and heat transfer enhancement caused by spacer grid in rod-bundle geometry. Gandhir and Hassan used Reynolds-averaged Navier-Stokes (RANS) based turbulence model for single-phase CFD analysis of flow in pressurized water reactor (PWR) assemblies [1]. Liu et al. implemented several readily available turbulence models in order to determine the model most suitable for the flow [2, 3]. Navarro and Santos used the k-ε model to perform flow simulations with the CFD code in a PWR 5 × 5 rod bundle segment with a split-vane spacer grid [4]. Conner et al. conducted experiments to validate the CFD methodology for the single-phase flow conditions in pressurized water reactor (PWR) fuel assemblies [5]. Holloway et al. showed that there was a great variation of heat transfer distribution along a fuel rod due to the spacer grid type [6, 7]. A series of four-subchannel CFD simulations to analyze the heat transfer enhancement in a fully heated rod bundle with vane spacers were performed by In et al. [8]. By adjusting model coefficients adopted in a quadratic k-ε model, Baglietto and Ninokatahad previously have shown the promising capability of the RSM turbulence model in sufficiently accurate anisotropy modeling of the wall shear stress distribution and the velocity field in tight lattice fuel bundles [9]. Házi had demonstrated that the RSM could be accurately applied in simulating the rod bundle geometry [10].

To the best of the authors' knowledge, most of the CFD works are focusing on the hydraulic characteristics in the rod

Table 1: Projected areas of a mixing vane and a guide tap.

	Mixing vane (mm^2)	Guide tap (mm^2)
Grid Design 1	6.745	12.544
Grid Design 2	6.745	16.908

bundles with inner straps spacer grids but less attention had been paid to the hydraulic characteristics in the rod bundles with outer strap grids. In this study, four quarter-bundles from neighboring fuel assemblies are used to analyse the influence of spacer grid outer strap on fuel assembly thermal hydraulic performance. To be a reference, subchannel analysis is conducted by using FLICA, a subchannel analysis code.

2. CFD Modeling

2.1. Grids Description. In present study, two kinds of outer straps with the same inner straps were assembled and were used to investigate the influences of outer straps on the thermal hydraulic performance. As shown in Figure 1, grids of Design 1 and Design 2 have different outer strap designs. Design 2 has a guide tap on each of intersecting joints of outer strap and inner strap, but Design 1 has a guide tap on every other intersecting joint. The guide tap of Design 2 is much wider and lower than that of Design 1. Moreover, Design 2 has holes on the center of outer strap. The projected areas of mixing vane and guide tap are listed in Table 1, since the Design 2 has much more guide taps and the guide tap has larger projected area and the projected area of Design 2 is larger than that of Design 1.

2.2. Computational Domain and Mesh. To simulate the outer straps' influence between fuel assemblies downstream, four quarter-bundles from neighboring fuel assemblies are constructed to form the computational domain as shown in Figure 2(a). The diameter of rod is 9.5 mm, and the pitch is 12.6 mm. The inlet length before entering the grid is 50 mm, and the outlet length after leaving the grid is 522 mm (take the bottom face of the grid as reference plane). Consequently the total length of the flow domain as shown in Figure 2(b) is 572 mm.

Nonstructure tetrahedral mesh element is utilized in the grid region due to the complex geometry that consisted of springs and dimples of spacer grid. The application of extruded prism type mesh in the flow passage region may reduce the number of mesh elements and offer a better mesh quality. The mesh element size was elaborate setup for a good response of the detailed structure inside the grid. The total number of mesh element is up to 30 million.

2.3. Simulation. The simulation is based on a single-phase model and steady state condition. The physical parameters of water are calculated from IAPWS-IF97 code under 15.5 MPa, 310°C condition as constant and the flow is considered to be incompressible.

The mesh number of each simulation is more than 30 million. The boundary conditions in this calculation are listed in Table 2. The Reynolds number in the fuel bundle could reach up to 500,000 under the above condition. The RNG k-ε model which is less sensitive to the mesh and boundary condition was utilized in this simulation. The simulation is performed on a IBM high performance computation blade server with 128 cores for half an hour to get a steady converged solution, and the total 500 iterations were required to get this solution.

Table 2: Boundary conditions.

Boundary	Option	Value
Inlet	Uniform normal velocity	4.737 m/s
	Uniform temperature	310°C
Outlet	Relative static pressure	0 Pa
Periphery interface	Translational periodicity	
Grid	Nonslip wall, adiabatic	
Rod	Nonslip wall, wall heat flux*	

*The power distributions of rod bundle are showed in Figure 3.

3. Results and Discussion

3.1. Pressure Drop. Pressure drop of a grid is a very important parameter. If the pressure drop increases, the lift force will need to be adapted. As shown in Figure 4, the pressure drop of Design 2 is about 6.9% larger than that of Design 1. This is due to the large projected area of Design 2, which causes more coolant to be blocked.

3.2. Lateral Flow. Lateral flow intensity is evaluated by the cross-sectional averaged lateral flow and is defined as

$$V_{\text{lateral}} = \sqrt{V_u^2 + V_v^2}, \tag{1}$$

where V_u, V_v are the cross-sectional averaged lateral velocity in directions X and Y. It is seen, in Figure 5, that the lateral flows of both Design 1 and Design 2 gradually increase before flowing into the grids and reach the maximum when coolant just leaves the grids, and then the cross-flow decreases gradually. Comparing the differences of lateral flow between the two grids, Design 1 has relatively smaller lateral flow upstream of the grid but a relatively larger lateral flow downstream of the grid.

The upstream and downstream lateral flows have different flow mechanisms. The lateral flow upstream is driven by flow redistribution induced by different subchannel pressure loss coefficient. As pointed out in the geometric illustration of Designs 1 and 2, the only difference is the outer strap structure, major in the guide tap geometrical characteristics, leading to different subchannel pressure loss coefficient distribution within the grids. In addition, according to Section 3.1, the side subchannel pressure loss coefficient of Design 2 is larger than that of Design 1, leading to more uneven flow distribution and stronger lateral flow.

While in the downstream, the lateral flow is mainly driven by mixing vane at the location very near to the grids downstream edge and that is the reason why Design 1

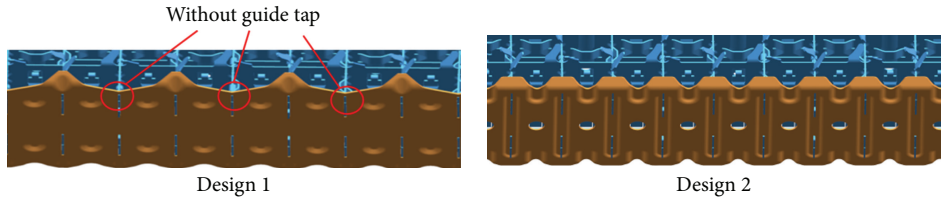

(a) (b)

Figure 1: Schematic illustration of outer strap.

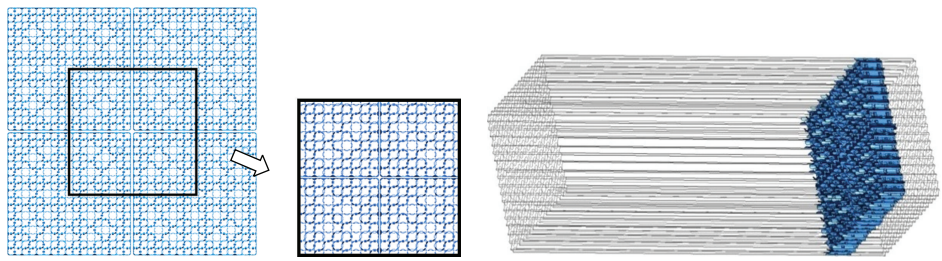

(a) (b)

Figure 2: Computational domain and mesh.

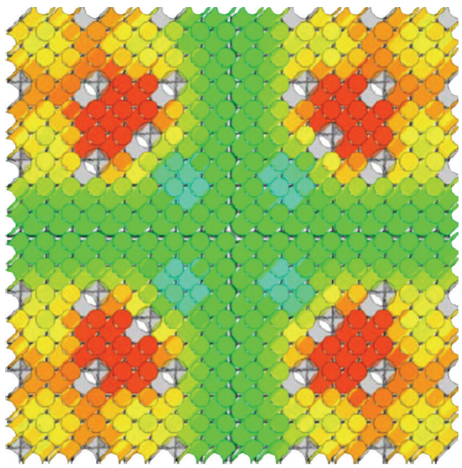

Figure 3: Power distributions.

and Design 2 have the same lateral flow intensity at this location. As shown in Figure 5, lateral flow induced by Design 2 is smaller than that induced by Design 1 in the downstream, showing the effect of reduced lateral flow of Design 2 compared to Design 1. Figure 6 shows the lateral flow velocity profile on each cross-sectional downstream grid. As presented in Figures 6(a)–6(c), lateral flow induced by Design 1 is much stronger than that induced by Design 2 in the region of the outer strap, which indicates that more lateral flow is blocked by Design 2 compared to Design 1.

3.3. Cross Bundle Flow. According to lateral flow analysis in Section 2.2, the two designs have obviously different flow patterns near side channels. To further analyze the influence of outer straps on lateral flow, streamlines are created to obtain information about the coolant lateral spreading over the downstream of the grid. Figures 7(a)–7(e) shows streamline development, from grid upstream to outlet, of the coolant flow in near outer strap region and the red color is the top-down view of the subchannel investigated. The distance of the coolant spread on the lateral is showed on the top-down view of the streamline. Figures 7(a)–7(b) show that the coolant downstream the Design 1 has a stronger mixing because the intensity and extent of cross bundle flow induced by Design 1 are stronger than those induced by Design 2. Moreover, it is also noted that the geometrical effect of grid on lateral flow is usually limited within a 3 subchannel lateral distance downstream in axial flow travel of one span distance. Inside grids, the two grids have the similar flow pattern downstream.

Figure 8(a) shows that clip planes, numbered from 1 to 9, are created to quantitatively analyze the cross bundle flow at different axial location. Each clip plane is 50 mm high. The mass flow pass through each clip plane is calculated to analyze the cross bundle flow variation, shown in Figure 8(b). It is seen that the cross bundle mass flow gradually decreases as the flow develops downstream the grids. It can also be seen that the cross bundle mass flow of the Design 1 is much more than that of Design 2.

3.4. Temperature Distribution. Temperature distribution at the outlet is studied by CFX but also by a subchannel analysis code, FLICA, in present study. Figure 9 presents the subchannel-averaged temperature distribution at the outlet of one-quarter grid by using CFX. According to the structure characteristic, the grid is divided into 4 types of subchannels,

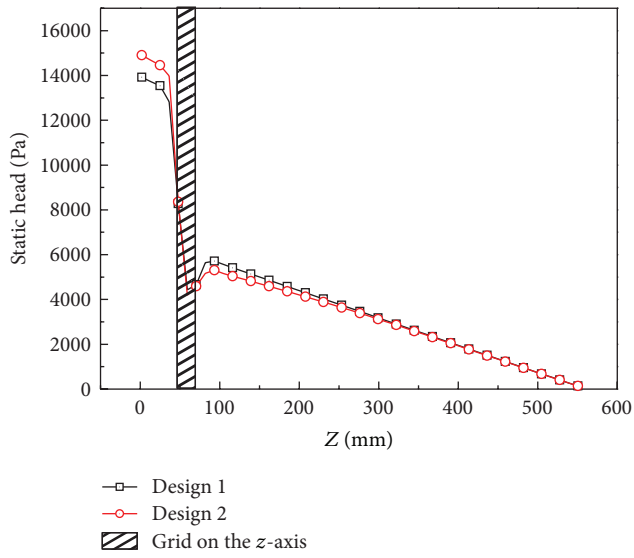

Figure 4: Pressure drop.

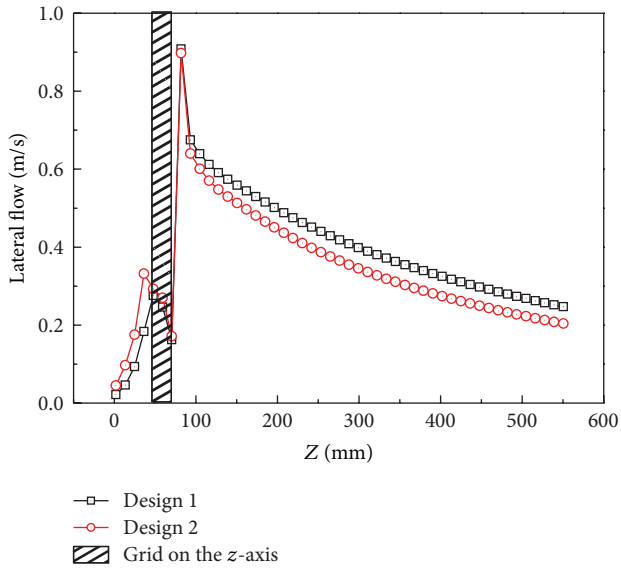

Figure 5: Lateral flow intensity.

side subchannels (green), guide thimble subchannels (yellow), typical subchannels (white), and Conner subchannel (blue). As shown in Figure 9, the hottest channel of the two grid appears at the side subchannels.

The CFX calculation result shows that the outlet temperature standard deviation is 0.477°C and 0.419°C for Design 2 and Design 1, respectively. Design 1 has a slightly smaller value compared to Design 2, meaning that the mixing effect of Design 1 is better than that of Design 2. The FLICA calculation result shows that the outlet temperature distribution is proceeding to more uniform as the mixing coefficient increases for either Design 1 or Design 2, shown in Figure 10. It is interesting to note that FLICA result shows that Design 2 always has smaller outlet temperature standard deviation than Design 1 does, meaning that the mixing effect of Design 2 is better. This confliction of FLICA and CFX results leads us to do further investigation of the subchannel outlet temperature distribution. As the illustration of Design 1 and 2 geometry, the only difference is the outer strap structure, major in the guide tap geometrical characteristics, leading to different subchannel pressure loss coefficient distribution within the grids and the local flow field in the vicinity of side channels. In typical subchannel analysis code like FLICA, the influence of outer strap structure is taken into account in terms of pressure loss coefficient only, which means that the resultant effect of flow redirection caused by guide tabs cannot be calculated. In contrast, CFX calculation takes every detailed geometrical influence on the resulted flow into account, reflected by the temperature variation in Figure 11. Since the cross-section averaged temperatures calculated by FLICA and CFX are the same (within 0.15°C), it is reasonable to treat FLICA and CFX calculation as the right results in general, but CFX gives more detailed and reasonable temperature and flow distribution.

When we explore the outlet temperature distribution obtained by FLICA and CFX, it is interesting to note that the hottest channel presented by FLICA maintains the same for Design 1 and Design 2 at the same mixing coefficient, subchannel 26 when mixing coefficient equals to 0 and subchannel 16 for other mixing coefficients. Either subchannel 26 or subchannel 16 is a typical subchannel bounded by four fuel rods. However, the CFX calculation gives quite different results as expected. In CFX calculation, subchannel 37 is the hottest channel for Design 1 and subchannel 41 for Design 2, as shown in Figures 9(c)-9(d) and Figure 12. Subchannels 37 and 41 are side channels next to Design 1 outer strap and Design 2 outer strap, respectively. The CFX result clearly shows that the outer strap has a significantly impact on temperature distribution. It is also found that the temperature difference between FLICA and CFX for

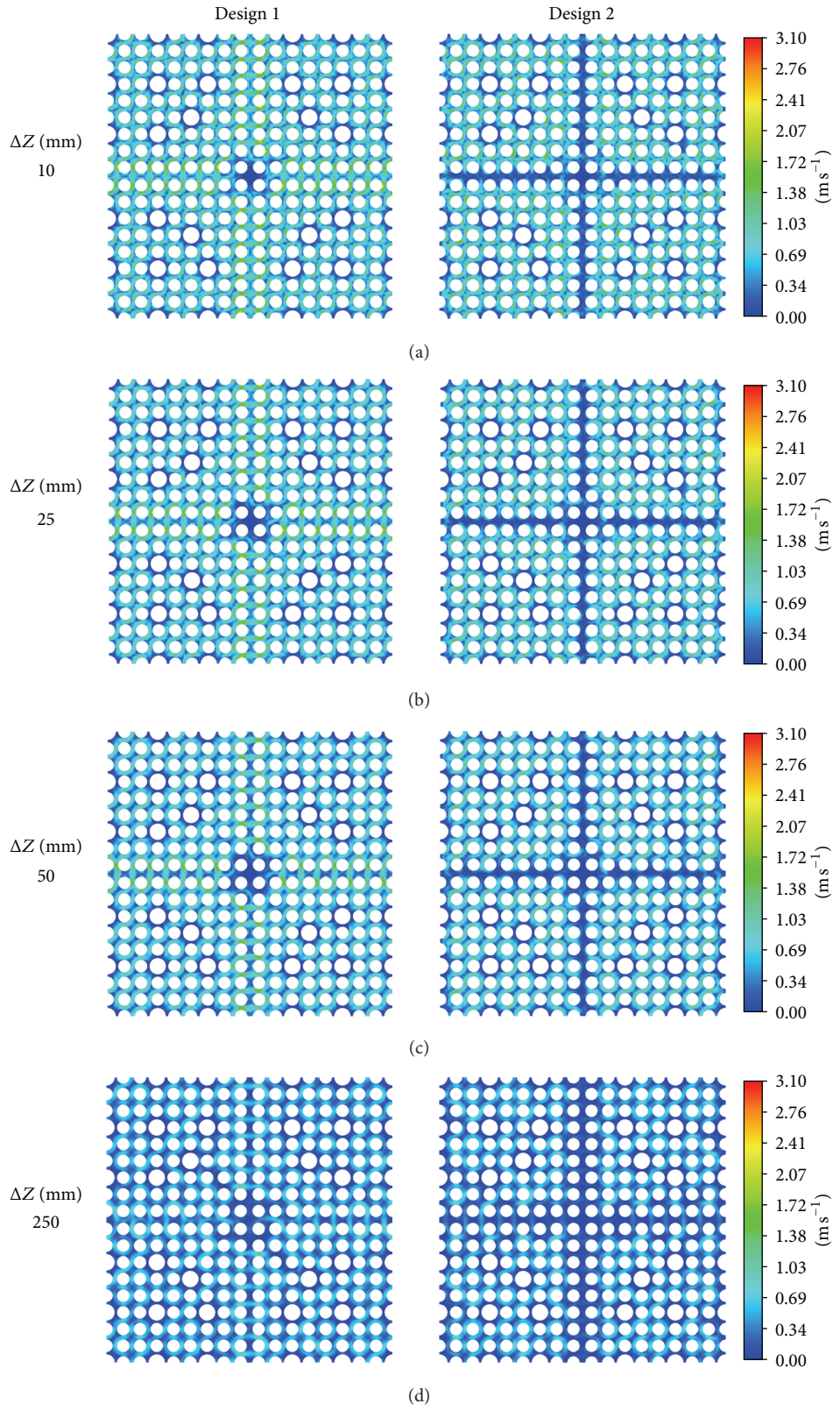

Figure 6: Lateral flow velocity profile (ΔZ is the distance from grid to the cross-section).

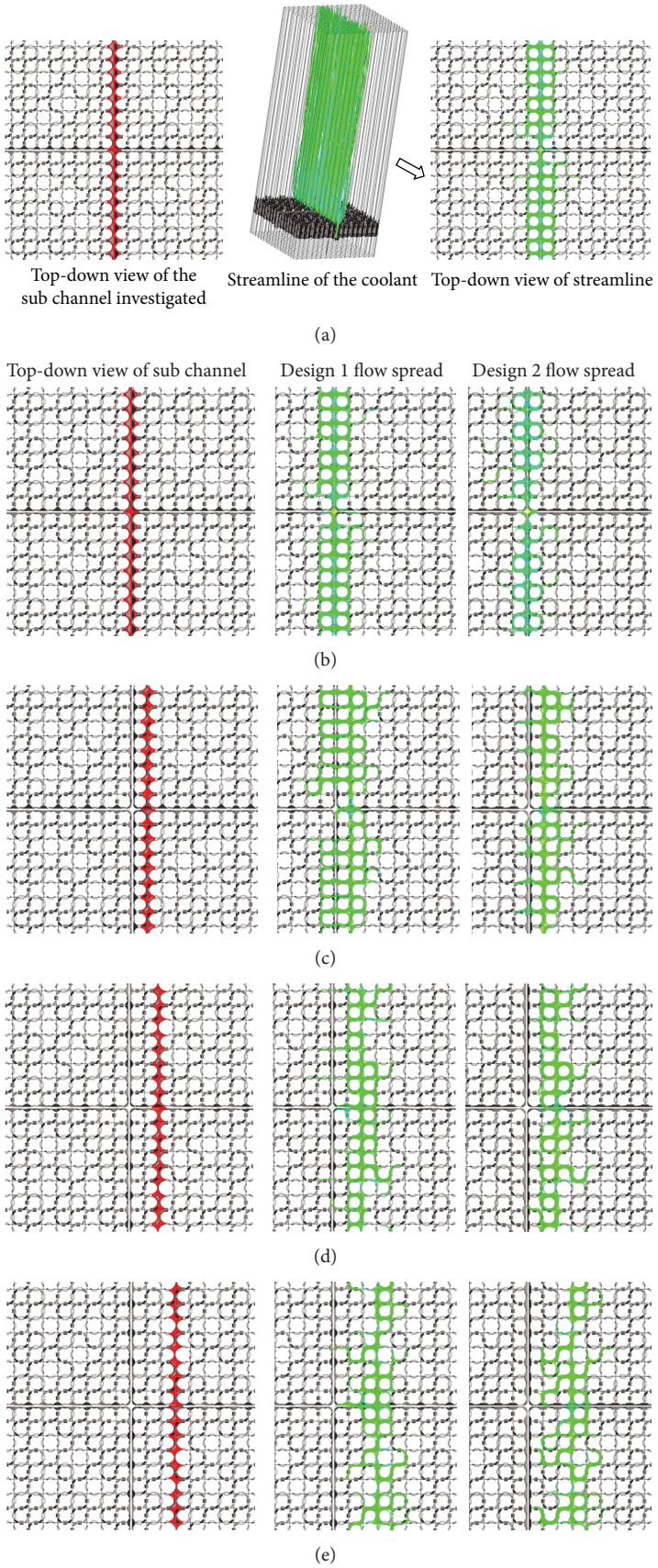

Figure 7: Top-down view of streamline at different subchannels near the outer strap.

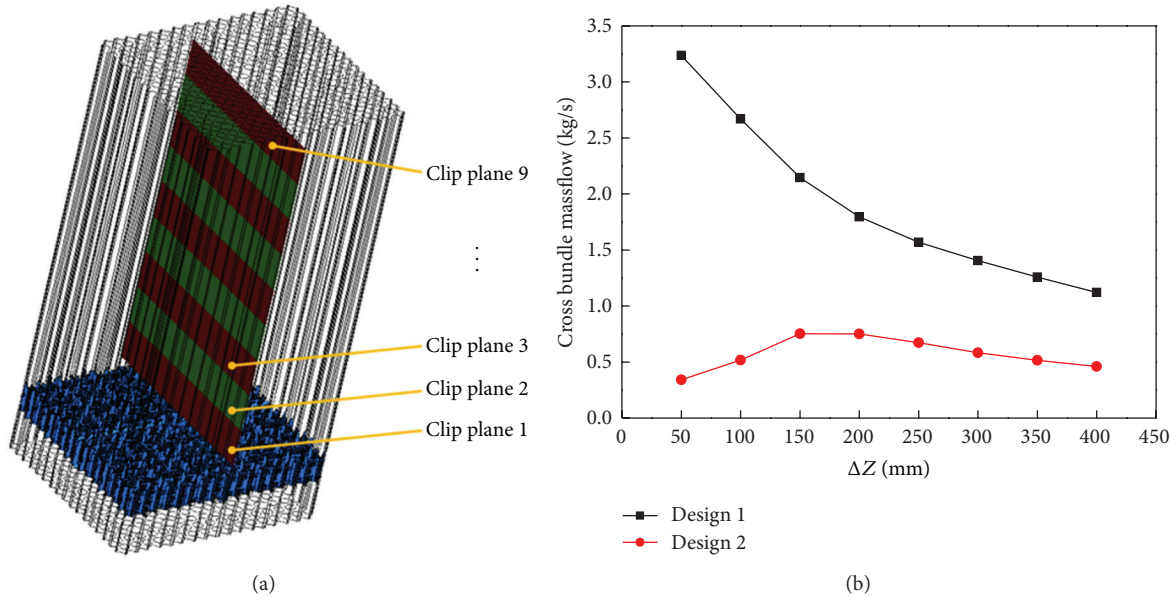

FIGURE 8: Cross-bundle mass flow at different axial location.

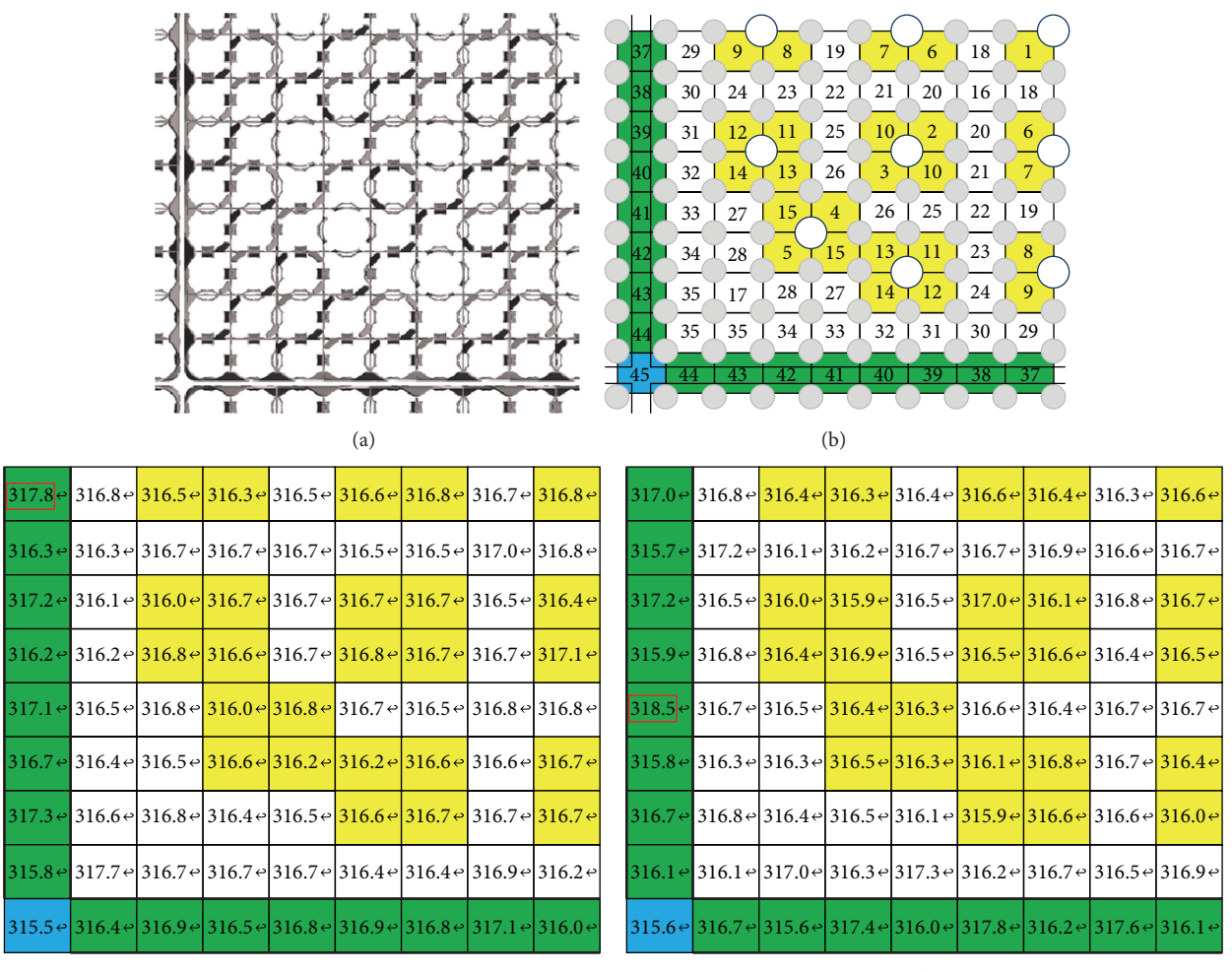

FIGURE 9: Subchannels outlet temperature: (a) outlet location; (b) subchannel numbering; (c) Design 1 temperature, CFX result; (d) Design 2 temperature, CFX result.

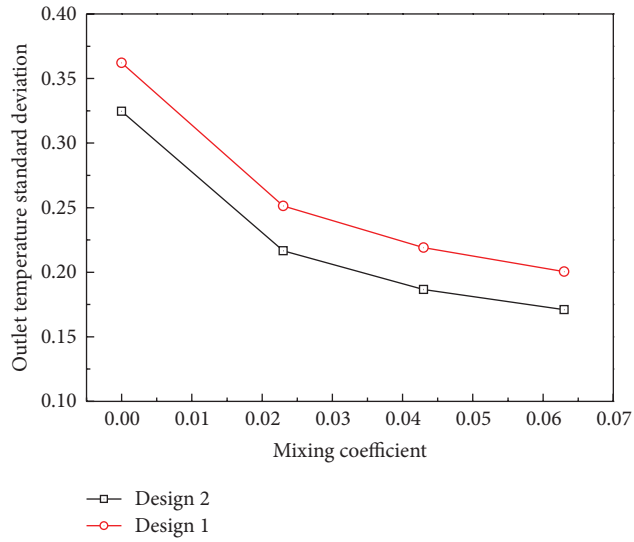

Figure 10: Outlet temperature standard deviation variation as mixing coefficient.

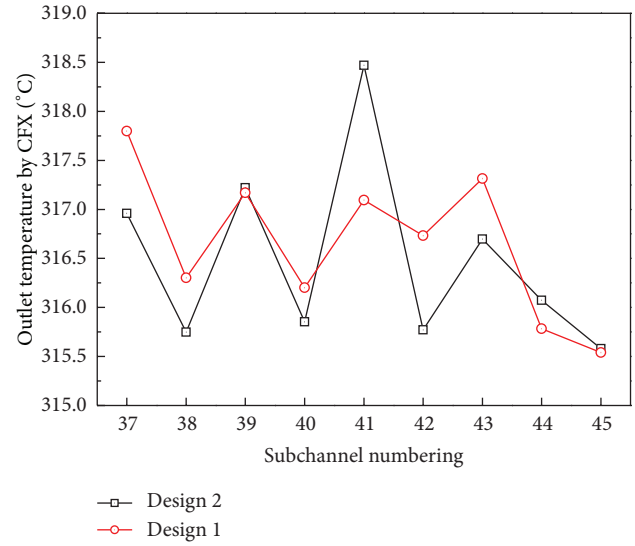

Figure 11: Side subchannel outlet temperature calculated in CFX for Design 1 & 2.

the hottest channel of Design 1, subchannel 37, is 1.6°C and for the hottest channel of Design 2, subchannel 41, is 2.2°C. Such big temperature difference (over 10% difference compared to the cross-section averaged temperature rise from inlet to outlet of ~6°C) between FLICA and CFX results, as well as the 0.7°C difference (or close to 12% variation over the 6°C temperature rise from inlet to exit) between the hottest channels of Design 1 and Design 2 obtained from CFX computation, clearly indicates that subchannel analysis code may miss some useful information in comparison with CFX analysis.

4. Concluding Remarks

Outer straps not only have important effect on enhancing grid mechanical strength and decreasing hang-up susceptibility but also have significant impact on grid thermal hydraulic performance such as grid pressure drop, lateral flow, and temperature distribution. Due to the larger flow block area of side subchannel of grid Design 2, the pressure drop of Design 2 grid is about 6.9% larger than that of Design 1. The larger side subchannel pressure loss coefficient changes the resistance distribution and subsequently results in larger lateral flow of Desgin 2 upstream but weaker lateral flow downstream due to the stronger blocking effect of the outer strap. In general, based on the comparison between CFX and FLICA, both computational fluid dynamic method and subchannel analysis code can give reasonable result in single-phase flow simulation, but the application of subchannel analysis code should be very careful because too much geometrical information has been omitted in typical codes.

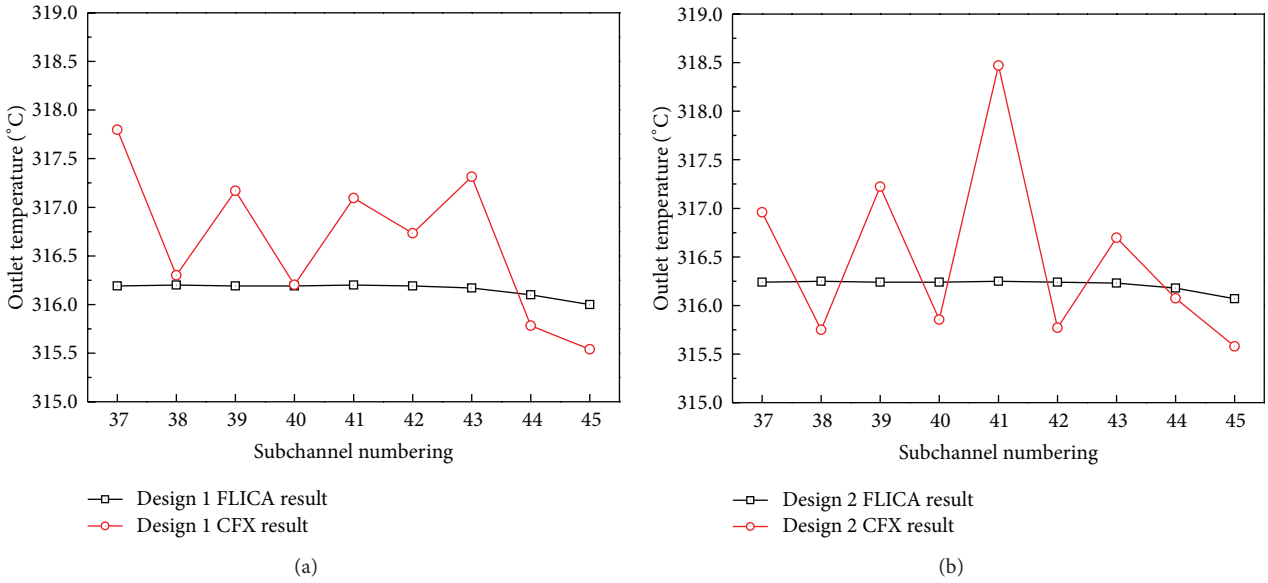

Figure 12: Side subchannel outlet temperature in CFX & FLICA (mixing coefficient equal to 0.063) calculation.

Conflict of Interests

The authors declare that there is no conflict of interests regarding the publication of this paper.

References

[1] A. Gandhir and Y. Hassan, "RANS modeling for flow in nuclear fuel bundle in pressurized water reactors (PWR)," *Nuclear Engineering and Design*, vol. 241, no. 11, pp. 4404–4408, 2011.

[2] C. C. Liu, Y. M. Ferng, and C. K. Shih, "CFD evaluation of turbulence models for flow simulation of the fuel rod bundle with a spacer assembly," *Applied Thermal Engineering*, vol. 40, pp. 389–396, 2012.

[3] C. C. Liu and Y. M. Ferng, "Numerically simulating the thermal-hydraulic characteristics within the fuel rod bundle using CFD methodology," *Nuclear Engineering and Design*, vol. 240, no. 10, pp. 3078–3086, 2010.

[4] M. A. Navarro and A. A. C. Santos, "Evaluation of a numeric procedure for flow simulation of a 5×5 PWR rod bundle with a mixing vane spacer," in *Proceedings of the International Nuclear Atlantic Conference (INAC '09)*, 2009.

[5] M. E. Conner, E. Baglietto, and A. M. Elmahdi, "CFD methodology and validation for single-phase flow in PWR fuel assemblies," *Nuclear Engineering and Design*, vol. 240, no. 9, pp. 2088–2095, 2010.

[6] M. V. Holloway, D. E. Beasley, and M. E. Conner, "Investigation of swirling flow in rod bundle subchannels using computational fluid dynamics," in *Proceedings of the 14th International Conference on Nuclear Engineering (ICONE '06)*, pp. 1–11, Miami, Fla, USA, July 2006.

[7] M. V. Holloway, D. E. Beasley, and M. E. Conner, "Single-phase convective heat transfer in rod bundles," *Nuclear Engineering and Design*, vol. 238, no. 4, pp. 848–858, 2008.

[8] W. K. In, T. H. Chun, C. H. Shin, and D. S. Oh, "Numerical computation of heat transfer enhancement of a PWR rod bundle with mixing vane spacers," *Nuclear Technology*, vol. 161, no. 1, pp. 69–79, 2008.

[9] E. Baglietto and H. Ninokata, "A turbulence model study for simulating flow inside tight lattice rod bundles," *Nuclear Engineering and Design*, vol. 235, no. 7, pp. 773–784, 2005.

[10] G. Házi, "On turbulence models for rod bundle flow computations," *Annals of Nuclear Energy*, vol. 32, no. 7, pp. 755–761, 2005.

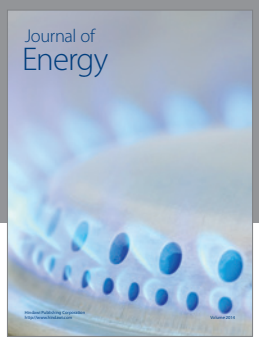

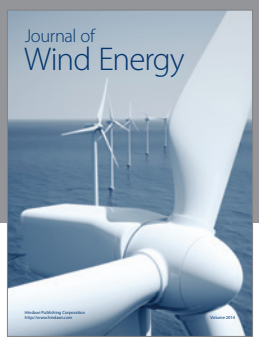

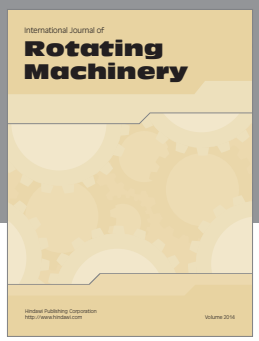

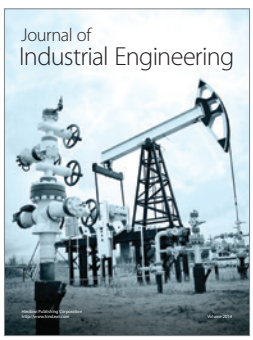

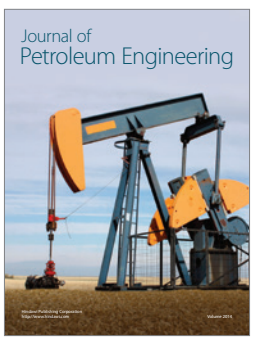
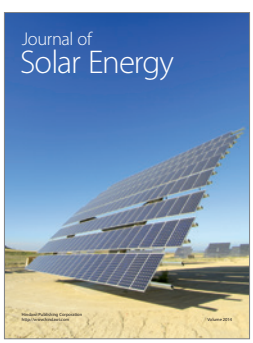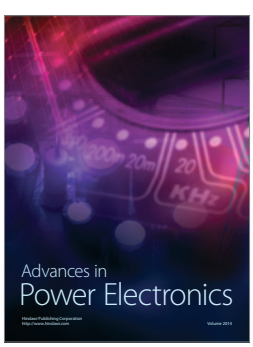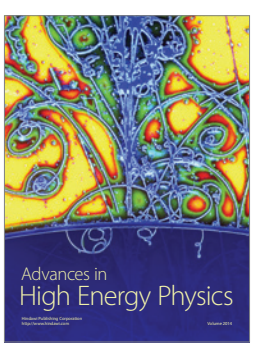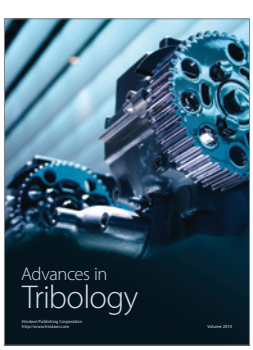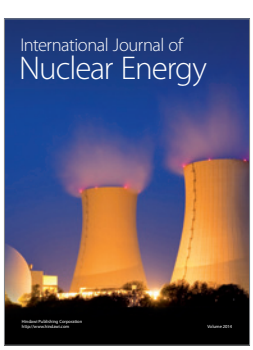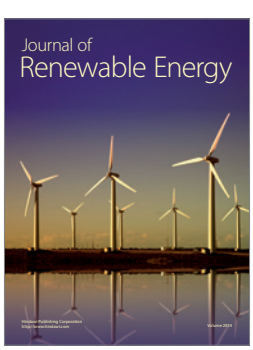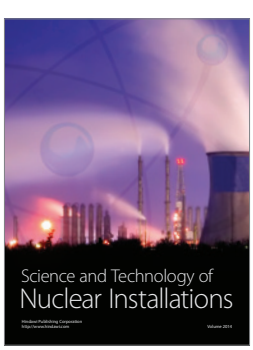
Hindawi
Submit your manuscripts at
http://www.hindawi.com